Environment International 146 (2021) 106283

Contents lists available at ScienceDirect

Environment International

journal homepage: www.elsevier.com/locate/envint

Immune cell profiles associated with measured exposure to phthalates in the Norwegian EuroMix biomonitoring study – A mass cytometry approach in toxicology

Unni C. Nygaard [a,*], Emilie S. Ulriksen [a], Hege Hjertholm [a], Friederike Sonnet [a,b], Anette K. Bølling [a], Monica Andreassen [a], Trine Husøy [a], Hubert Dirven [a]

[a] Department of Environmental Health, Norwegian Institute of Public Health, Lovisenberggata 8 Oslo, Norway
[b] Department of Parasitology, Leiden University Medical Center, Albinusdreef 2, 2333 ZA Leiden, Netherlands

ARTICLE INFO

Handling Editor: Lesa Aylward

Keywords:
Phthalates
Immunotoxicology
Immune cells
Mass cytometry
Biomarkers
Mechanisms

ABSTRACT

Background: Phthalate exposure has been associated with immune-related diseases such as asthma and allergies, but there is limited knowledge on mechanisms, effect biomarkers and thus biological support of causality.
Objectives: To investigate associations between exposure to the phthalates DEHP (di(2-ethylhexyl) phthalate) and DiNP (diisononyl phthalate) and functional immune cell profiles.
Methods: Peripheral blood mononuclear cells (PBMCs) from 32 healthy adult Norwegian participants in the EuroMix biomonitoring study were selected based on high or low (n = 16) levels of urine metabolites of DEHP and DiNP. High-dimensional immune cell profiling including phenotyping and functional markers was performed by mass cytometry (CyTOF) using two broad antibody panels after PMA/ionomycin-stimulation. The CITRUS algorithm with unsupervised clustering was used to identify group differences in cell subsets and expression of functional markers, verified by manual gating.
Results: The group of participants with high phthalate exposure had a higher proportion of some particular innate immune cells, including CD11c positive NK-cell and intermediate monocyte subpopulations. The percentage of IFNγ TNFα double positive NK cells and CD11b expression in other NK cell subsets were higher in the high exposure group. Among adaptive immune cells, however, the percentage of IL-6 and TNFα expressing naïve B cell subpopulations and the percentage of particular naïve cytotoxic T cell populations were lower in the high exposure group.
Discussion: Cell subset percentages and expression of functional markers suggest that DEHP and DiNP phthalate exposure may stimulate subsets of innate immune cells and suppress adaptive immune cell subsets. By revealing significant immunological differences even in small groups, this study illustrates the promise of the broad and deep information obtained by high-dimensional single cell analyses of human samples to answer toxicological questions regarding health effects of environmental exposures.

1. Introduction

The immune system is a fine-tuned and complex system, and dysregulation plays a fundamental role in a variety of diseases and conditions, including several non-communicable diseases (NCDs; (Davis et al., 2017)). Environmental pollution, such as synthetic and natural chemicals, have been shown to affect the development of immune diseases (Hessel et al., 2015; Kravchenko et al., 2015). However, immunotoxicological endpoints reflecting immune functions have only recently and to a limited extent been considered in regulatory risk assessments of chemicals. Identification of causal relationships as well as appropriate biological assays and biomarkers of effect to assess adverse effects on the immune system is in high demand. Such knowledge is required to motivate development and implementation of effective policies for reduced chemical exposure, and a subsequent reversion of the present increases in disease incidence and socioeconomic costs (EFSA CEF Panel (EFSA Panel on Food Contact Materials et al., 2019).

Phthalates are a group of chemicals commonly used as plasticizers,

* Corresponding author at: Norwegian Institute of Public Health, Pb 222-Skøyen, N-0213 Oslo, Norway.
E-mail address: unnicecilie.nygaard@fhi.no (U.C. Nygaard).

https://doi.org/10.1016/j.envint.2020.106283
Received 27 July 2020; Received in revised form 5 November 2020; Accepted 11 November 2020
Available online 2 December 2020

lubricants, and solvents in a variety of consumer products, such as food contact materials, building materials, cosmetics and toys (Luo et al., 2018; Wittassek et al., 2011). Due to their common use and wide range of applications, phthalates are ubiquitous environmental chemicals. Consequently, phthalate metabolites are present in all or most analyzed urine samples, this is especially evident for high molecular weight (HMW) phthalates that are present in higher levels (Husoy et al., 2019; U.S. Department of Health and Human Services, 2019). The urinary phthalate levels reflect the total phthalate exposure through ingestion, inhalation and dermal absorption, but for most HMW phthalates diet is considered to be the primary exposure route (Wittassek et al., 2011).

Human exposure to phthalates has been associated with immune diseases such as asthma and allergies (Agier et al., 2019; Bølling et al., 2020; Wu et al., 2020). The underlying cellular and molecular mechanisms are still not identified and effect biomarkers for phthalates in humans are limited (Baken et al., 2019; Bolling et al., 2013). Experimental studies provide support for immunological effects of phthalates. In mice, airway and oral exposure to di(2-ethylhexyl) phthalate (DEHP) results in airway inflammation or adjuvant effects indicative of sensitization, possibly due to a shift towards Th2 and Th17 responses and an expansion of follicular T helper cells (Tfh) (Alfardan et al., 2018; Guo et al., 2012; Han et al., 2014). Immunosuppressive effects of phthalates have also been reported, in terms of decreased phagocytic activity and inflammatory mediator release from macrophages, while increased release of Th2 mediators was reported from lymphocytes (Bølling et al., 2020).

The limited knowledge about mechanistic pathways and biomarkers of effect for phthalate exposure, which can also strengthen causality links, may be explained by the historical lack of methods to resolve the great complexity of the human immune system. Technological advancements now provide opportunities of single cell mass cytometry using CyTOF (Cytometry by Time Of Flight mass spectrometry), which permits simultaneous use of 40–50 metal isotope-tagged antibody specificities in a single tube (Bandura et al., 2009). Such high numbers of antibodies can detect cell surface markers defining cell subtypes and their activation status, and simultaneously also functional markers like intracellular cytokines, signaling pathways, activation and proliferation. Combined with unsupervised computational algorithms, mass cytometry data may discover cell profiles or subpopulations associated with exposure or disease. This approach is particularly powerful in identifying new cell subsets or combination of characteristics/markers that are easily overlooked in traditional (supervised) analyses (Amir el et al., 2013; Bendall et al., 2012, 2014; Vendrame et al., 2017).

The aim of the present exploratory study was to identify functional immune cell profiles, e.g. cell subpopulations or functional characteristics, associated with phthalate exposure. By combining the powerful CyTOF technology with peripheral mononuclear cell (PBMC) samples from participants in the well-characterized biomonitoring study within the EuroMix project, we performed immune cell profiling on selected participants with the highest and lowest urinary levels of the two phthalates DEHP and diisononyl phthalate (DiNP). These high-molecular weight phthalates were chosen because DEHP is one of the major phthalates with regard to exposure, also in the EuroMix study (Husoy et al., 2019), and with known effects on the immune system (Bølling et al., 2020). DINP is an industrial substitute for DEHP with similar structure, also demonstrating immune-related effects, such as cytotoxicity in vitro (Eljezi et al., 2019), autoimmune thyroid disease (Duan et al., 2019), and adjuvant effect on OVA-induced allergic airway inflammation in rats (Chen et al., 2015). This is the first study, to the best of our knowledge, demonstrating the usefulness of explorative high-dimensional single cell analysis by mass cytometry (CyTOF) in human samples in answering toxicological research questions regarding health effects of environmental exposures.

2. Material and methods

2.1. Study subjects and design

Adult subjects (25–64 yrs old) were selected from a Norwegian human biomonitoring study which was part of the EU EuroMix project, see (Husoy et al., 2019) for details. Inclusion criteria for the study were being adult between 18 and 70 years, with no diseases the last week before participation. The study was approved by the Norwegian Regional Committee for Medical and Health Research Ethics (REK ID no 2015/1868). Written, informed consent was obtained from all participants and all procedures were performed in accordance with approved guidelines.

2.2. Urinary phthalate measurements and selection of participants

For all 144 participants in the EuroMix cohort, urinary phthalate metabolite concentrations were determined in three pooled batches of urinary samples collected from 6 am-12 pm, 12 pm-6 pm and 6 pm-6 am (next morning) and kept at −80 °C until analyses. Urinary phthalate metabolite concentrations were determined by on-line column switching liquid chromatography coupled to tandem mass spectrometry (HPLC-MS-MS) as described elsewhere (Sabaredzovic et al., 2015). The mean value of the resulting urine metabolite concentrations from the three pools, measured to be over the limit of detection (LOD), was subsequently adjusted for specific gravity and averaged over the 24 h of collection. Results on cohort level are previously reported (Husoy et al., 2019).

After correction for molecular weight, all DEHP and DiNP metabolites for each individual were summed (∑DEHP and ∑DiNP). Individuals with high and low levels of ∑DEHP + DiNP were selected (n = 16, 8 females and 8 males; Fig. 1, Suppl Table S1). Correspondingly, high and low levels of the other phthalates, and phenols (Husoy et al., 2019), were considered, as well as aiming for as similar as possible age and body weight (group median).

2.3. Immune cell profiling by mass cytometry

At the end of the 24 h reporting period, blood samples were collected with EDTA anti-coagulant. Peripheral blood mononuclear cells (PBMCs) were isolated by Ficoll separation as previously described (Sonnet et al., 2020), within one hour after collection and preserved in liquid nitrogen.

After thawing, each sample was stained with two different metal-conjugated antibody panels (Table 1) to perform a deep and broad immune cell phenotyping of unstimulated cells (Panel 1) and assess functional characteristics of cellular subpopulations after stimulation with

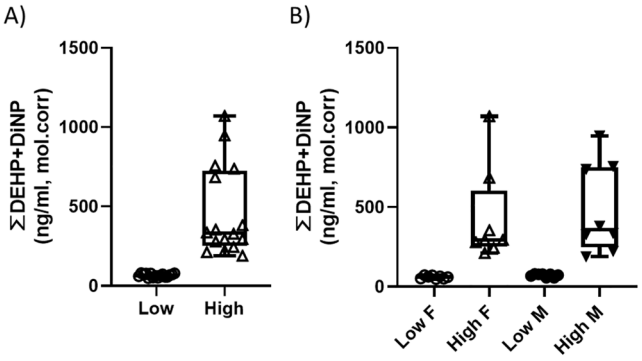

Fig. 1. Urine levels of the sum of DEHP and DiNP (sum of the urinary metabolites corrected for molecular weight, ∑DEHP + DiNP) in the two defined groups of participants with low and high exposure (A, n = 16), also stratified by sex (B, n = 8, F = female, M = male)). Dots denote the value per individual, while the boxes denotes the group median and interquartile range values.

Table 1
Mass cytometry antibody panels. Metal isotope tags, antibody target, clones and provider used for staining of unstimulated cells (Panel 1) and stimulated cells (Panel 2). * used for clustering in the CITRUS algorithm for abundancy, # for median marker expression. Below the dotted line, markers for cell identification and viability.

Panel 1				Panel 2			
Metal isotope	**Target**	**Clone**	**Provider**	**Metal isotope**	**Target**	**Clone**	**Provider**
Surface markers				**Surface markers (2A)**			
141Pr	CD196 (CCR6)*	11A9	Fluidigm	142Nd	CD19 #	HIB19	Fluidigm
142Nd	CD19*#	HIB19	Fluidigm	143Nd	CD127/IL-7Ra	AD19D5	Fluidigm
143Nd	CD127 (IL-7Ra)*#	A019D5	Fluidigm	145Nd	CD4 #	RPA-T4	Fluidigm
144Nd	CD69	FN90	Fluidigm	147Sm	CD11c #	Bu15	Fluidigm
145Nd	CD4*#	RPA-T4	Fluidigm	148Nd	CD16 #	3G8	Fluidigm
146Nd	IgD*#	TA6-2	Fluidigm	153Eu	CD185/CXCR5 #	RF8B2	Fluidigm
147Sm	CD11c*#	Bu15	Fluidigm	154Sm	CD3 #	UCHT1	Fluidigm
148Nd	CD16*#	3G8	Fluidigm	155Gd	CD45RA #	HI100	Fluidigm
149Sm	CD194 (CCR4)*	205,410	Fluidigm	158Gd	CD33	WM53	Fluidigm
150Nd	CD134 (Ox40)	ACT35	Fluidigm	164Dy	CD23	EBVCS-5	Fluidigm
151Eu	CD123 (IL-3R)*#	6H6	Fluidigm	166Er	BAFF-R/CD268		BioLegend
152Sm	γδTCR*#	11F2	Fluidigm	167Er	CD197/CCR7 #	G043H7	Fluidigm
153Eu	CD185 (CXCR5)*	RF8B2	Fluidigm	168Er	CD8 #	SK1	Fluidigm
154Sm	CD3*#	UCHT1	Fluidigm	169Tm	CD25/IL-2R #	2A3	Fluidigm
155Gd	CD45RA*#	HI100	Fluidigm	170Er	HLA-DR #	L243	Fluidigm
156Gd	CD183 (CXCR3)*	G025H7	Fluidigm	173Yb	CD154/CD40L		BioLegend
158Gd	CD33*#	WM53	Fluidigm	174Yb	CD161		BioLegend
159Tb	CD161	HP-3G10	Fluidigm	175Lu	CD14 #	M5E2	Fluidigm
160Gd	CD28	CD28.2	Fluidigm	176Yb	CD56 #	NCAM16.2	Fluidigm
162Dy	CD27*#	L128	Fluidigm	89Y	CD45	HI30	Fluidigm
163Dy	CD294 (CRTH2)*	BM16	Fluidigm	**Intracellular markers (2B)**			
164Dy	CD23	EBVCS-5	Fluidigm	144Nd	IL-2	MQ1-17H12	Fluidigm
165Ho	CD163	GHI/61	Fluidigm	150Nd	IL-22	22URTI	Fluidigm
166Er	CD24*#	ML5	Fluidigm	151Eu	IL-5	TRFK5	Fluidigm
167Er	CD197 (CCR7)*	G043H7	Fluidigm	152Sm	TNFα	Mab11	Fluidigm
168Er	CD8a*#	SK1	Fluidigm	156Gd	IL-10	JES-9D7	BioLegend
169Tm	CD25 (IL-2R)#	2A3	Fluidigm	159Tb	IL-13	JES10-5A2	BioLegend
170Er	HLA-DR*#	L243	Fluidigm	161Dy	IL-17A	BL168	Fluidigm
171Yb	IL-33R /ST2*#	Sf21	R&D systems	162Dy	Foxp3 #	259D/C7	Fluidigm
172Yb	CD38*#	H1T2	Fluidigm	163Dy	IL-4	MP4-25D2	Fluidigm
173Yb	CD371*	50C1	Fluidigm	165Ho	IFNγ	B27	Fluidigm
174Yb	IgG*#	MNK-49	BioLegend	171Yb	IL-6	MQ2-BA5	BioLegend
175Lu	CD14*#	M5E2	Fluidigm	172Yb	IL-21	3A3-N2	Fluidigm
176Yb	CD56*#	NCAM16.2	Fluidigm				
209Bi	CD11b*	ICRF44	Fluidigm				
089Y	CD45	HI30	Fluidigm				
191Ir	Cell-ID		Fluidigm	191Ir	Cell-ID		Fluidigm
193Ir	Cell-ID		Fluidigm	193Ir	Cell-ID		Fluidigm
195Pt	Cisplatin, live/dead		Fluidigm	195Pt	Cisplatin, live/dead		Fluidigm

Phorbol 12-myristate 13-acetate (PMA) and ionomycin (Panel 2).

Panel 1 consisted of 36 antibodies targeting surface markers. This panel was designed to identify the major cell populations in PBMCs (T-cells (including Th- and Tc-cells), B-cells, NK-cells, Monocytes (Mo) and dendritic cells (DC)), numerous subpopulations and the expression of activation markers and costimulatory molecules. Panel 2 was used to stain stimulated cells and consisted of 20 antibodies targeting surface molecules and 12 antibodies targeting intracellular proteins. Panel 2 was designed to identify the major immune cell populations mentioned above, as well as regulatory T cells and intracellular cytokine production. Metal-tagged antibodies were obtained from Fluidigm (CA, USA) or Biolegend (CA, USA; see Table 1) and conjugated in house using Maxpar® X8 Antibody Labelling Kits (Fluidigm) according to the manufacturer's instruction. The in-house conjugated antibodies were diluted based on titration performance in Candor PBS-based Antibody Stabilization solution (Candor Biosciences, Germany) and stored at 4 °C. For the cytokine antibodies, a mass minus many (MMM) control was performed to confirm that any detected cytokine production was neither due to spillovers from other channels nor background noise.

Cells were thawed and the samples prepared for mass cytometry according to descriptions in Sonnet et al. (2020). In short, PBMCs were gently thawed in benzonase-containing medium, washed, counted, and two vials each of 3 million cells were left to rest over night at 37 °C in a CO_2 incubator. Cells in one of the two vials were stimulated for 4 h (CO_2 incubator, 37 °C) with 20 ng/mL PMA and 1 μg/mL ionomycin. Brefeldin A (BFA) was added to a concentration of 10 μg/mL. Both aliquots were washed, incubated with Cisplatin as a viability marker, and stained with the surface marker panels (unstimulated aliquot with Panel 1 and the stimulated aliquot with Panel 2A). After washing, the stimulated aliquot was fixed, permeabilized with methanol and left overnight at −20 °C, before being rehydrated and stained with the antibody cocktail for the intracellular markers (Panel 2B). Ir191/193 intercalators were used for all samples to identify cells (distinguished from debris). After washing, the cells were left pelleted until mass cytometry analyses the same day.

The CyTOF data were acquired on a CyTOF II instrument (Fluidigm) equipped with a SuperSampler system [Victorian Airship & Scientific Apparatus]. Immediately before data acquisition, cells were resuspended in Maxpar® Water (Fluidigm) to a concentration of 2.5–5 $*10^5$ cells/mL, and EQ™ Four Element Calibration Beads (Fluidigm) added to give a 1:10 dilution. Filtered suspensions were acquired at a rate of 300–600 events/second.

2.4. Data analyses

All files were normalized using the Fluidigm CyTOF Software 6.7 for Windows (Fluidigm). Subsequent data and statistical analyses were performed with Cytobank software (Cytobank Inc., CA, USA) and GraphPad Prism 7 (GraphPad Software, Inc.). Living single CD45+ cells were selected for all downstream analysis by manual biaxial gating

excluding doublets (based on DNA (Ir191/193) content and event length), EQ beads, cisplatin-containing dead cells, and non-existing double positive cells (CD19+ CD3+ and CD19+ CD14+). (Suppl. Fig. S1)

With an explorative aim, we used the CITRUS algorithm (cluster identification, characterization, and regression (Bruggner et al., 2014)) to identify populations and patterns of interest. CITRUS first uses an unsupervised data-driven hierarchical clustering algorithm, including files from all participants, to identify clusters of cell subpopulations based on the marker expressions, displaying a hierarchy of phenotypically related cell clusters. Secondly, the relative cell abundance and/or median marker expression of these clustered populations were compared between the two groups of low and high ∑DEHP + DiNP exposed individuals, the association models returning the features that have statistically significant differences between samples in different groups for a given cluster. Due to the explorative character of the study and the relatively small groups, we report both results from the correlative, non-parametric test SAM (significant analysis of microarrays, FDR of 5%) model and from the predictive models PAMR (R implementation of prediction analysis of microarrays) or LASSO (L1-Penalized Regression) (Grace and Nacheva, 2012; Tibshirani, 1996; Tibshirani et al., 2002; Van der Laan et al., 2003). In our case, the model error rate plots for the predictive models usually were not good, however, the characteristics for the clusters identified by CITRUS as being part of the set of nodes statistically significant between the groups were still used as a starting point for further investigations.

All CITRUS analyses were performed three times on the same data set but with independent down-sampling. While the results reported are from the first run, only results being reproduced in all three CITRUS runs are highlighted. For cell clusters identified as significantly different between groups by CITRUS, we focused on the cell node furthest down in the hierarchy, to identify the "purest" cluster. Data from these cell clusters were further investigated, by performing pairwise comparison between the cell abundance and/or mean marker intensities by Kruskal-Wallis test (KW; high versus low exposure group) and Mann-Whitney with Dunn's multiple comparison post-hoc test (MW; high and low exposed groups stratified by sex), using GraphPad Prism.

For all main findings, manual gating of populations with the most important characteristics (marker expression) was performed, and results compared between groups. The main motivation for this manual gating was to confirm that the results were robust, and even with a smaller set of markers. Such "verification" with fewer markers will allow future studies to apply higher throughput (flow cytometry) methods in their study design to detect the relevant subpopulations/putative biomarkers of effect.

CITRUS analysis was performed on living intact single cells with the default configuration (arcsinh cofactor = 5, normalize = "global", sampling of 5000 random evets per file, down-sampling exclusion percentile = 0.01, target number of clusters = 250, maximum number of clustered events = 50000) and a 2% cutoff for cluster size. For the statistical models, a false discovery rate (FDR) of 5% and global normalization scales were used. For the predictive models, results from analyses with cv_min are presented, i.e. corresponding to the model with the fewest number of features necessary to have the lowest cross validation (cv) error rate. For unstimulated cells (Panel 1), clustering was performed on i) all 35 markers (excluding CD45) and ii) 27 phenotyping markers (marked * in Table 1) excluding clearly functional/activation markers (CD69, CD23, CD25, CD28, CD134/Ox40, CD371, CD163, CD161) and CD45. Median expression of the activation markers HLA-DR, CD69, CD23, CD25, CD28, CD134/Ox40, CD11b, CD371 and CD163 were compared between the groups after clustering on 21 main phenotyping markers (marked # in Table 1). For stimulated cells (Panel 2), clustering was performed using i) all 30 markers (excluding CD45, and CD33 due to an artefact "upregulation" of this marker in stimulated cells) and ii) 14 phenotyping markers (marked * in Table 1). Differences between groups for median expression for the 11 cytokines and the activation markers CD23, CD25, HLA-DR, CCR7 and the costimulatory marker CD154 were investigated, after clustering on the same 30 and 14 markers.

For data visualization purposes, viSNE (visualization of t-Distributed Stochastic Neighbour Embedding (Amir et al., 2013). was performed on living CD45+ singlets including data from all participants, with the default configuration (in Cytobank; seed: (random), # iterations: 1000, perplexity: 30, theta: 0,5). Unless otherwise noted, all markers (except CD33 for stimulated cells, see below) were used for clustering and 4000 events (or the maximum available for the B and T subsets) were sampled from each individual.

3. Results

3.1. Immune cell profiles associated with phthalate exposure levels in unstimulated cells

While clustering on all 35 markers did not result in conclusive analyses for either SAM, PAMR or LASSO, clustering performed on the 27 surface/phenotyping markers only (i.e. excluding CD45 since used for pre-gating and the activation markers CD69, CD25, CD23, CD134/Ox40, CD28, CD371, CD163 and CD161) provided several consistent results.

Several branches of CD56+ (NK cell marker) cell clusters were identified as being increased in the high ∑DEHP + DINP exposed group (PAMR analyses; Fig. 2A). The NK#1 cell cluster, characterized as an activated NK cell subpopulation based on its high expression of CD56, CD11c and CD161 (also being CD45RA++ CD38++ CD16+ CCR7- CD8- CD27-, Suppl. Fig. S2), tended to be increased in the high ∑DEHP + DINP exposed group (non-significant in Kruskal-Wallis test but the trend were apparent in both sexes (data not shown)). The increase of this activated NK cell population was confirmed to be significant after manual gating of CD3- CD19- CD56+ CD45RA++ CD38++ CD16+ CD11c+ cells (Fig. 2B), apparent in both sexes (Fig. 2C), providing a strengthening of the result from the unsupervised gating.

The NK#2 cell cluster, CD56+ CD8+ CD3- CD19- CD11c- CD16+ (Suppl. Fig. S2) probably showed a trend of increase mainly driven by a single high sample, and the same pattern was observed after manual gating of CD19- CD3- CD56+ CD16+ CD8+ cells (data not shown). The NK#3 cell cluster was only marginally different between the two exposure groups and were not further investigated. Manual gating determining the % NK cells (CD56+ main population) or the % CD56bright CD16-/dim population did not show any differences between the two groups, while narrow gating of the CD56+ CD16+ NK cell populations were significantly increased in the high exposure group (Fig. 2D).

Another group of cell nodes identified in the PAMR analyses was a group of monocytes (Mo) showing slightly higher (n.s. in KW) levels in the high ∑DEHP + DINP exposed group. The Mo#1 was CD14+ CD16+ HLADR++ CD11b++ CD11c++ (CD123++ CD33+ CD38+, Suppl. Fig. S2), thus characterized as enriched for intermediate Mo according to Thomas et al., (Thomas et al., 2017). Also after manual gating of Mo (% of living CD45+ cells), a trend of higher % of Mo were seen in the high exposed group, and apparent in both sexes (Fig. 2E and F, respectively). After manual gating, percentages of nonclassical, classical, and intermediate Mo (according to Suppl. Table S2) reflected the % Mo when expressed as % of cells, while no group differences were seen when expressed as % of Mo. This indicates that the increase in Mo was driven by the different subgroups of Mo. The % of manually gated plasmacytoid dendritic cells (pDC) and myeloid (m) DC (according to Suppl. Table S2) did not differ between the groups (data not shown).

A cluster of naïve cytotoxic T cells (Tc#1, CD3+ CD8+ CD45RA++ CXCR3+ CD27++ CD294+ (variable expression), CCR7++ CD38+ IL-33R+ CD127+, Suppl. Fig. S2) had lower abundance in the high compared to the low ∑DEHP + DINP exposed group, in the SAM analyses. Investigating the abundance in this cluster, it was close to significant in KW analyses (Fig. 3A) and appeared to be driven by trends in

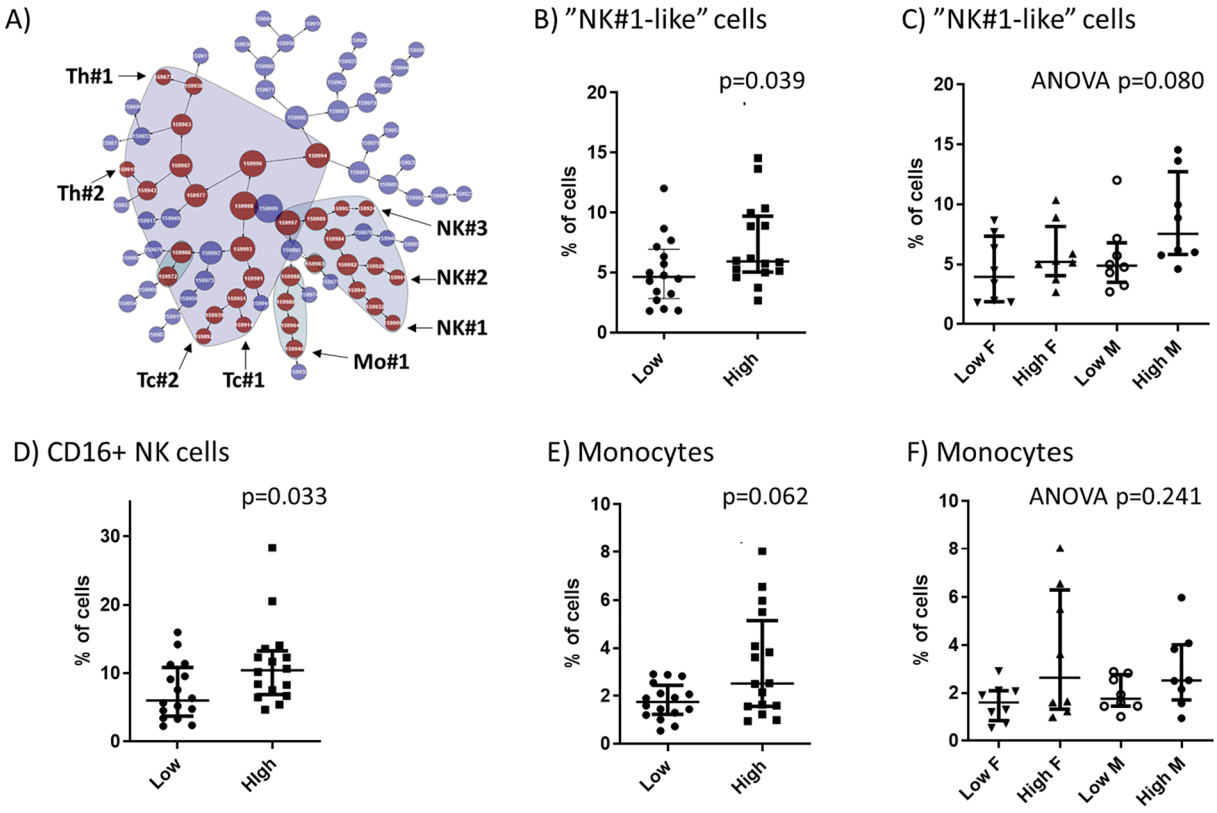

Fig. 2. NK cells and Monocytes in PBMCs from participants with low and high ∑DEHP + DINP exposure levels, determined in unstimulated cells stained with Panel 1 antibodies. (A) The CITRUS tree with cell cluster nodes, with red nodes denoting the minimum number of features necessary for group prediction of samples in the PAMR analyses. (B) Proportion of manually gated CD3- CD19- CD56+ CD45RA++ CD38++ CD16+ CD11c+ NK cells, (C) also stratified by gender. (D) Proportion of manually gated CD56+ CD16+ NK cells (gating strategy in Suppl. Fig. S1B) (E) Proportion of manually gated monocytes (according to Suppl. Table S2), (F) also stratified by gender. All populations are expressed as proportion of living singlet CD45+ cells. Dots denote the value per individual, while the lines denote the group median and interquartile range values. p-values shown are from nonparametric analyses. (For interpretation of the references to color in this figure legend, the reader is referred to the web version of this article.)

both sexes (Fig. 3B). Also, naïve Tc cell clusters (including Tc#1) were consistently showing up in the PAMR analyses (Fig. 2A). Manual gating of naïve (CD45RA++) Tc cells being CD27++ CXCR3+ CD127+ (with or without CD294+ gate) (Fig. 3C and D) were only showing a non-significant trend of lower levels in the high exposed group, possibly driven by high values for two individuals. Manual gating of the parent populations, % Tc or % naïve Tc cells did not show group differences (data not shown).

Subpopulations of naïve Th cells were consistently identified as reduced in the PAMR analyses, although the effect was weak, not significant in KW analyses and appeared to be driven by two individuals with high values in the low ∑DEHP + DINP exposed group (Fig. 3E). Similar results were seen after manually gating of Th and naïve Th cells (data not shown).

After clustering based on 21 phenotyping markers, median expression of the nine activation markers (HLA-DR, CD69, –23, −25, −28, −11b, −132/Ox40, −163 and −371) were compared between groups. While SAM revealed no differences, PAMR and LASSO identified some cell clusters differing between the high and low exposed groups. First, increased expression of CD11b was indicated on three different NK cell branches (CD8+ CD11c+ CD38++, CD8dim CD11c+ CD38++ and CD8dim CD11c dim CD38+ populations; Suppl. Fig. S3), confirmed significant in KW analyses (Fig. 4 A, B, C respectively) and trends were observed in both sexes (data not shown). The increased CD11b expression on NK cells was confirmed after manual gating, as significantly increased % of CD11b+ NKs (Fig. 4D), the trend was observed in both sexes (data not shown). Secondly, increased expression of CD25 in a branch of cell clusters were indicated. This cluster appeared to contain both T helper memory cells (CD4+ CD45RA- CD127+) and other cell types (HLA-DR+ CD38+), and no group differences were observed after manual gating of T-effector memory (TEM) cells, therefore this result is not further reported.

3.2. *Immune cell profiles associated with phthalate exposure levels in stimulated cells*

Clustering based on all 30 markers of Panel 2 revealed that a group of NK cells (CD56+ CD11c+ CD45RA++ CD16- CD161+/-; Suppl. Fig. S3) expressing various amounts of IFNγ and TNFα (being negative for IL-6 and the other cytokines investigated) were present at higher frequencies in the high versus the low ∑DEHP + DINP group (CITRUS SAM analyses; illustrated by NK#a, Fig. 5A, B and C). Some of these NK cells were weakly CD8+, as also seen in unstimulated cells stained with Panel 1. The abundancy of this cell cluster was significantly different between the two groups (Fig. 5B), and this trend was observed in both sexes (Fig. 5C), but were not confirmed after manual gating of TNFα IFNγ double positive NK cells. Significant group differences for a large family of NK cell clusters were confirmed in the PAMR analyses (Fig. 5A and data not shown). Manual gating of the parent population, i.e. NK cells (CD3- CD19- CD56+), in both the stimulated (data not shown) and unstimulated did not show clear group differences until stratifying for sex, then males showed a trend of increase in % of NK cells (% of true cell population) in the high exposure group (Fig. 5D). viSNE plots, and biaxial plots based on these manually gated NK cells, illustrate how subpopulations of the NK cells are expressing both IFNγ and TNFα (Fig. 5E and F, respectively).

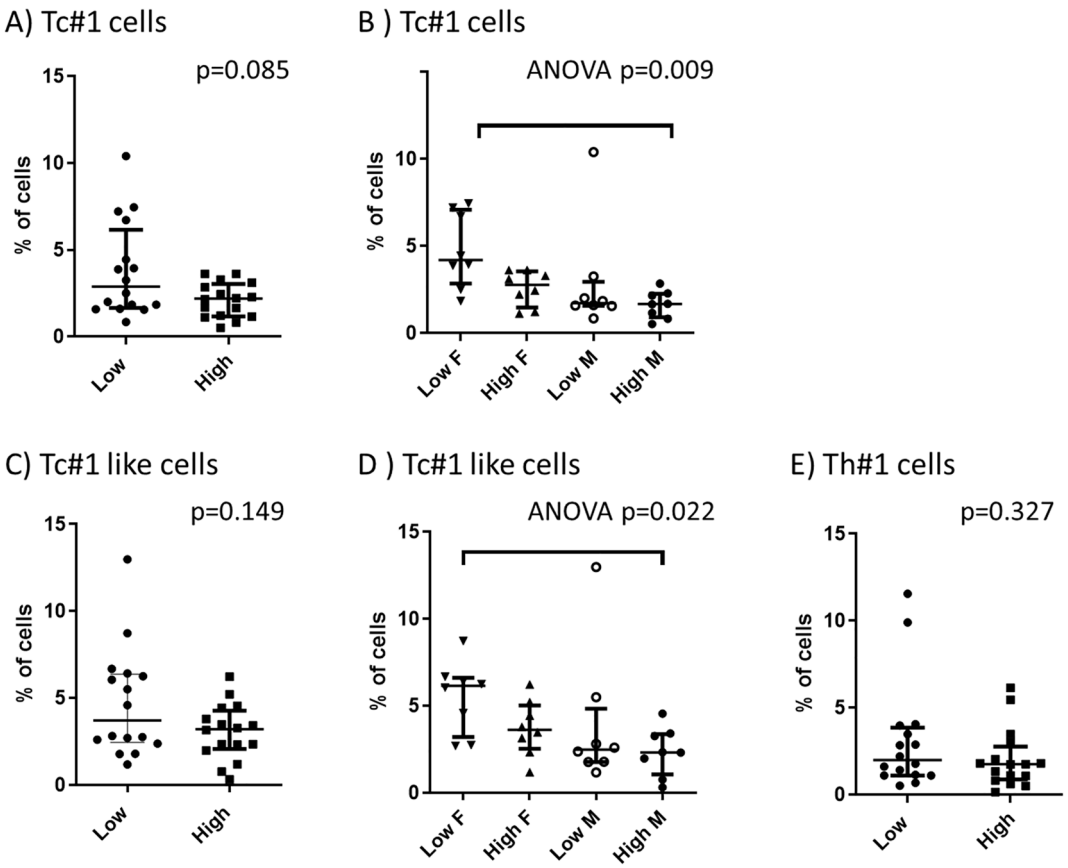

Fig. 3. T cells in PBMCs from participants with low and high ∑DEHP + DINP exposure levels, determined in the unstimulated cell sample stained with Panel 1 antibodies. (A) Proportion of cells in the Tc#1 node identified in the CITRUS analyses, (B) also stratified by sex. (C) Proportion of manually gated naïve Tc cells (CD3+ CD8+ CD45RA++) being CD27++ CXCR3+ CD127+, (D) also stratified by sex. (E) % of cells in the Th#1 node identified in the CITRUS analyses. All populations are expressed as proportion of living singlet CD45+ cells. Dots denote the value per individual, while the lines denote the group median and interquartile range values. p-values shown are from nonparametric analyses.

CITRUS PAMR analyses (clustered using the 30 markers, Fig. 5A) also pointed to group differences for the abundancy of a number of other cell clusters, characterized as Tfh, Tc, Th and B cell subpopulations (Fig. 5A, Suppl. Fig. S4). The B cell clusters with lower abundancy in the high exposed group were characterized as a naive B cell producing IL-6 and TNFα (B#a; CD19+ BAFFR+ CD45RA++ CXCR5++ CCR7dim HLADR++CD25+ IL-6+, TNFα+, all other markers neg; Suppl. Fig. S4). The reduction for the B#a cluster was not significant in KW (Fig. 6A), but evident after manual gating, seen as significantly lower % of TNFα and IL-6 double positive B cells (out of B cells) in the high ∑DEHP + DINP exposed group (Fig. 6B), showing a trend of reduction in both sexes (data not shown). The viSNE plots in Fig. 6E (run on B cells only) illustrates that TNFα is expressed in a limited subpopulation of the B cells, confirming that these cells are also CD19+ BAFFR+ CXCR5+. Further, it illustrates that the IL-6 expression in B cells was not restricted to TNFα + populations.

The proportion of a single cell cluster characterized as Thf (Thf#a Fig. 5A; CD3+ CD4+ CXCR5+ CD45RA- CD25+ CCR7+ CD161dim/+ TNFα + IFN-/dim, CD8-; Suppl. Fig. S4) were identified in PAMR from the first CITRUS run, as slightly decreased in the high ∑DEHP + DINP exposure group. This was not significant in KW statistics of the cell numbers in the single node, nor confirmed in two later CITRUS runs or after manual gating of T cells or Th cells being CXCR5+ or CXCR5+ CCR7+ (data not shown).

Two cluster families of Th cells and a cluster family of Tc cells also showed up in the PAMR analyses (Fig. 5A), with trends of decreased abundancy in the high ∑DEHP + DINP exposure group. The "end" clusters in these groups were characterized as Th#a, Th#b and Tc#1, but all clusters were only weakly reduced, not verifiable in KW analyses and were not further explored (data not shown). The direction of the changes, however, support the findings for Tc and Th cell subsets observed in unstimulated cells.

No median marker expression was significantly different between the two groups when doing CITRUS with clustering on all 30 markers and comparing groups by SAM or PAMR. In the LASSO analyses, however, a B cell cluster (CD19+ HLA-DR+ BAFF-R+ CD45RA+ CCR7med CXCR5+; Suppl. Fig. S5) showed significantly decreased expression of both IL-6, TNFα (Fig. 6C and D) and IL-10 (IL-10 expression was very low, data not shown), with similar trends for both sexes (data not shown). Clustering on 14 phenotyping markers only, these observations were confirmed (data not shown). This strengthen the observations of reduced abundancy of an IL-6 + TNFα + naïve B cell population reported above.

4. Discussion

By applying functional high-dimensional single-cell analyses, this exploratory study identified potential effect biomarkers and mechanisms for the reported associations between phthalate exposure and immune-related health outcomes. Within a Norwegian adult population with relatively low phthalate urine levels but comparable to other European cohorts (Husoy et al., 2019; Wang et al., 2019), the group with high DEHP and DINP exposure levels consistently had a higher proportion of several innate immune cell subpopulations, i.e. some particular NK-cell and monocyte subpopulations. Particularly consistent were the findings for IFNγ TNFα double positive NK cells and CD11c-

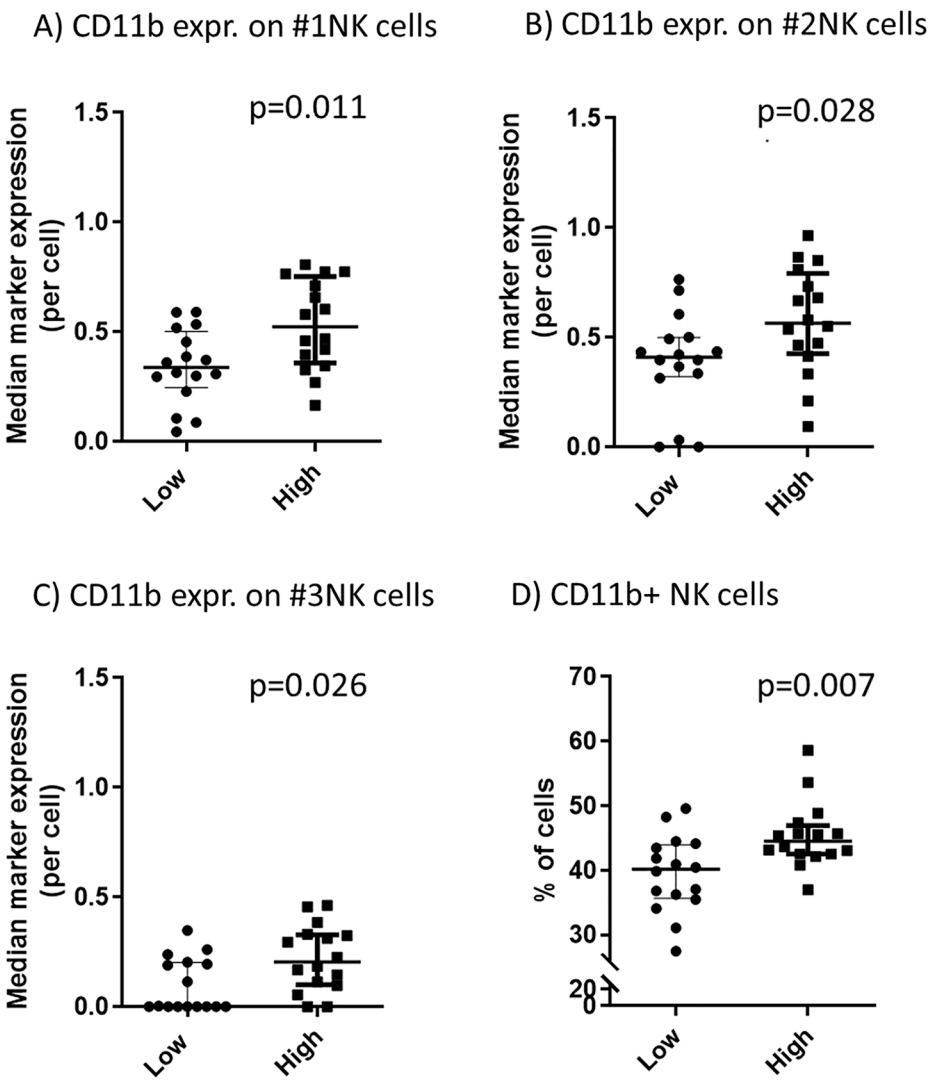

Fig. 4. NK cells in PBMCs from participants with low and high ∑DEHP + DINP exposure levels, determined in the unstimulated cell sample stained with Panel 1 antibodies. Median expression of CD11b per cell in the #1NK (A), #2NK (B) and #3NK (C) cell nodes identified by PAMR in CITRUS (expressed as % of living singlet CD45+ cells). (D) Proportion of CD11b+ NK cells (expressed as % of NK cells) determined after manual gating. Dots denote the value per individual, while the lines denote the group median and interquartile range values. p-values shown are from nonparametric analyses.

expressing NK subsets. For the adaptive immune cells, however, the % of particular subpopulations were lower in the high DEHP and DiNP exposure group, including IL-6 TNFα double positive B cell subpopulations and less consistently various naïve cytotoxic and helper T cell populations. An overview of the major findings is given in Fig. 7. To the best of our knowledge, this is the first study to exploit the power of high-dimensional mass cytometry analysis to identify biological changes associated with exposure to environmental xenobiotics. The novel cell populations and markers reported to be associated with phthalate exposure, however, need verification in larger studies or experimental studies for establishing causal relationship.

In spite of small group sizes (n = 16, 8 females and 8 males), several functionally distinct clusters of cells were consistently identified in repeated CITRUS analyses. Although not always statistically significantly different between the two groups using Kruskal-Wallis for that particular cell cluster, we used the CITRUS results to identify populations of interest. Based on their marker expression pattern, manual gating confirmed group differences for a number of these populations, between the groups with high and low ∑DEHP + DINP phthalate exposure. This confirmatory analysis increases the strength of the results using a smaller set of markers, also suggesting a set of markers suitable for use in future studies with higher throughput methods like flow cytometry. Only results confirmed by manual gating are discussed in the following.

The most consistent finding was higher abundance of NK cell populations expressing CD11c and CD16 in the group having high versus low exposure levels of ∑DEHP + DINP. This was detected by the unsupervised cluster analyses of both the unstimulated and stimulated sample, confirmed by manually gating on CD11c + NK cells as well as by significantly higher expression per cell of the maturation marker CD11b (Freud et al., 2006) on several NK cell clusters. To our knowledge this is the first study to report putative effects of phthalates on NK cells (Bølling et al., 2020). Expression of CD11c on NK-cells has been suggested to represent an activation-induced NK-cell population in autoimmune diseases like multiple sclerosis and diabetes (Aranami et al., 2006; Barcenilla et al., 2019), and CD11c+ NK cells were expanded and activated by circulating factors from trauma patients (Cahill et al., 2020). Furthermore, CD56+ CD16+ CD11c+ activated NK cell populations have been reported to have properties such as IFNγ production, tumor cell cytotoxicity, and the capability of inducing γδT lymphocyte proliferation (Li et al., 2013). An activated state was supported by the increased co-expression of IFNγ and TNFα from these NK cells after PMA/ionomycin stimulation. CD11b+ CD27- NK cells often have high cytolytic function and the high expression level of CD16 may suggest that the NK cell subpopulations identified in our study can be efficient mediators of antibody-dependent cellular cytotoxicity (Fu et al., 2014). Many of the cells in these NK cell populations expressed CD161, an indicator of a pro-inflammatory state in which these cells are able to respond to cytokines and contribute to inflammatory disease development (Kurioka et al., 2018). Both frequency and activation state of NK

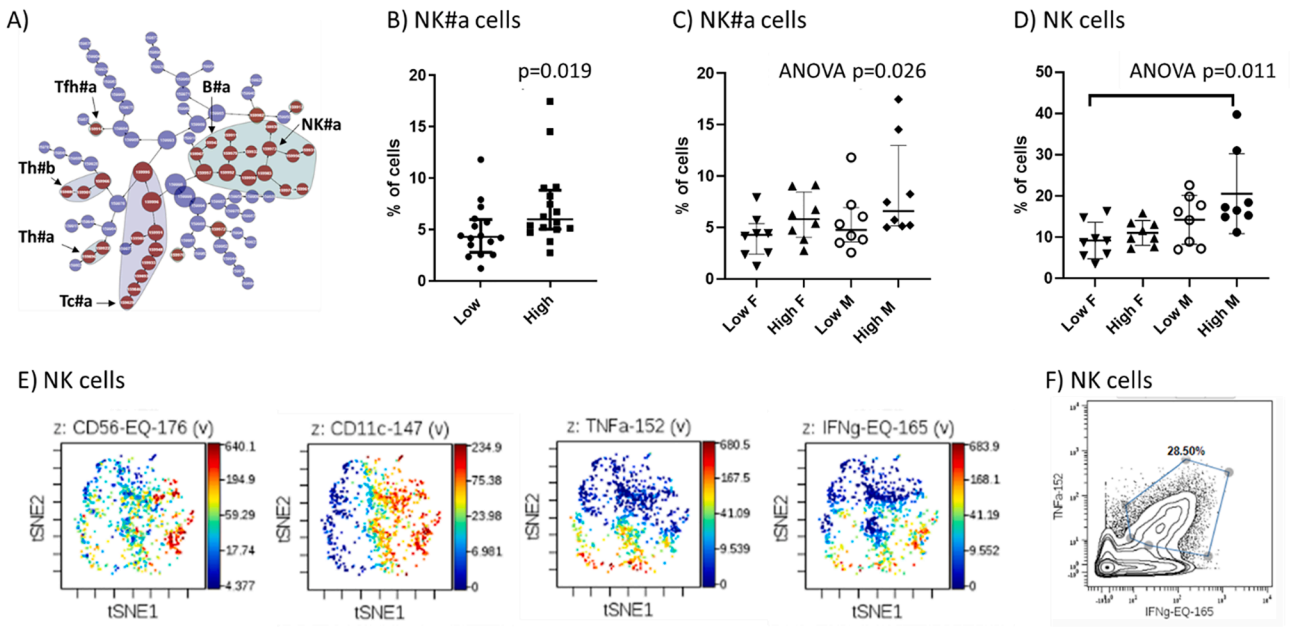

Fig. 5. Results from PBMCs from participants with low and high ∑DEHP + DINP exposure levels, stimulated for 4 h with PMA/ionomycin, and stained with Panel 2 antibodies. (A) The CITRUS tree with cell cluster nodes, with red nodes denoting the set of cell clusters necessary for group prediction of samples in the PAMR analyses (B) percentage of cells in the NK#a node identified in the CITRUS analyses (C) also stratified by sex. (D) Proportion of manually gated NK cells (CD3-CD19-CD56+) stratified by sex. All populations are expressed as % of living singlet CD45+ cells. Dots denote the value per individual, while the lines denote the group median and interquartile range values (E) viSNE plots from one participant, color codes showing expression of selected markers on a single cell level. The viSNE map was built using all 30 markers and data from all participants. (F) Biaxial plot including NK cell gate only, illustrating the presence of IFNγ + TNFα + double positive NK cells after manual gating, plot for one participant is shown. (For interpretation of the references to color in this figure legend, the reader is referred to the web version of this article.)

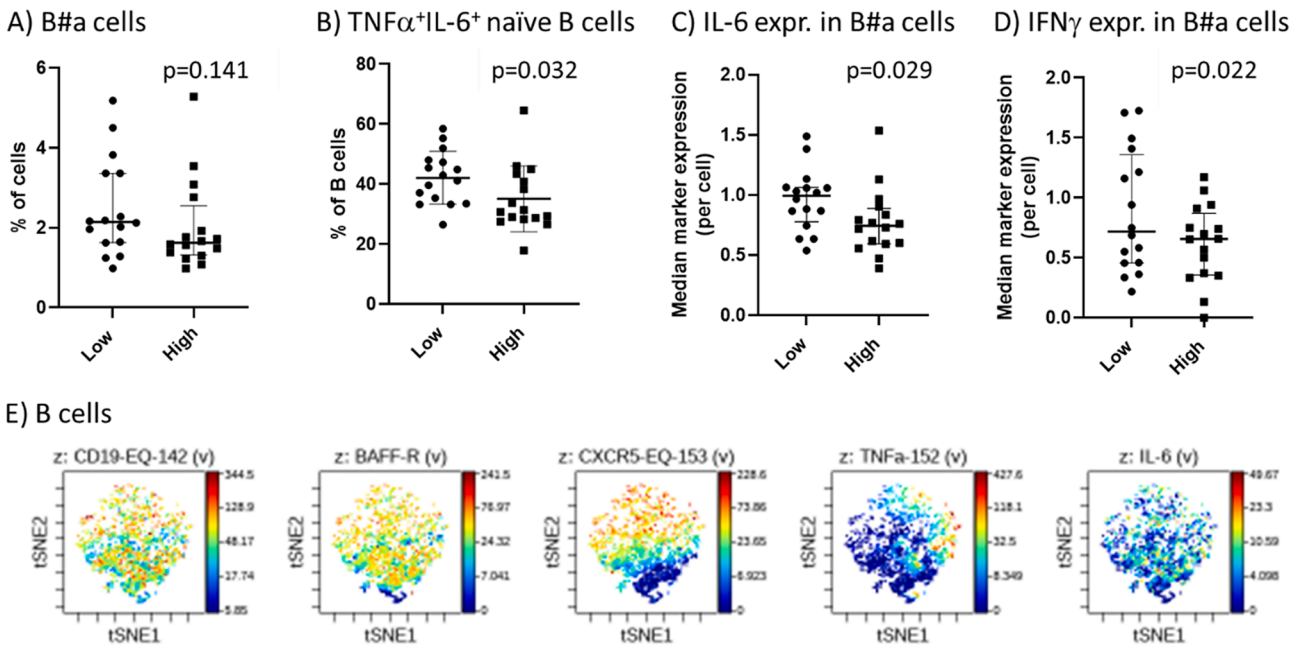

Fig. 6. B cells in PBMCs from participants with low and high ∑DEHP + DINP exposure levels, stimulated for 4 h with PMA/ionomycin, and stained with Panel 2 antibodies. (A) Proportion of cells in the B#a node from the CITRUS analyses (expressed as % of living singlet CD45+ cells) (B) proportion of manually gated B cells being double positive for IL-6 and TNFα (expressed as % of B cells). (C) and (D) show the median expression levels of IL-6 and IFNγ, respectively, in the B#a cell cluster. Dots denote the value per individual, while the lines denote the group median and interquartile range values. p-values shown are from nonparametric analyses. E) Illustrates the expression patterns of selected markers after performing a viSNE analyses including only B cells (CD3- CD19+ cells).

cells have been reported to be altered in a number of autoimmune diseases and HIV-infected patients (Michel et al., 2016; Mahapatra et al., 2019). Taken together, our data suggest that phthalate exposure may promote activated and pro-inflammatory NK cell populations with IFNγ and TNFα co-production, possibly of a cytolytic character.

Monocytes appeared to be elevated in a number of the individuals being exposed to high ∑DEHP + DINP levels, both as cell clusters characterized as intermediate Mo after unsupervised clustering and after

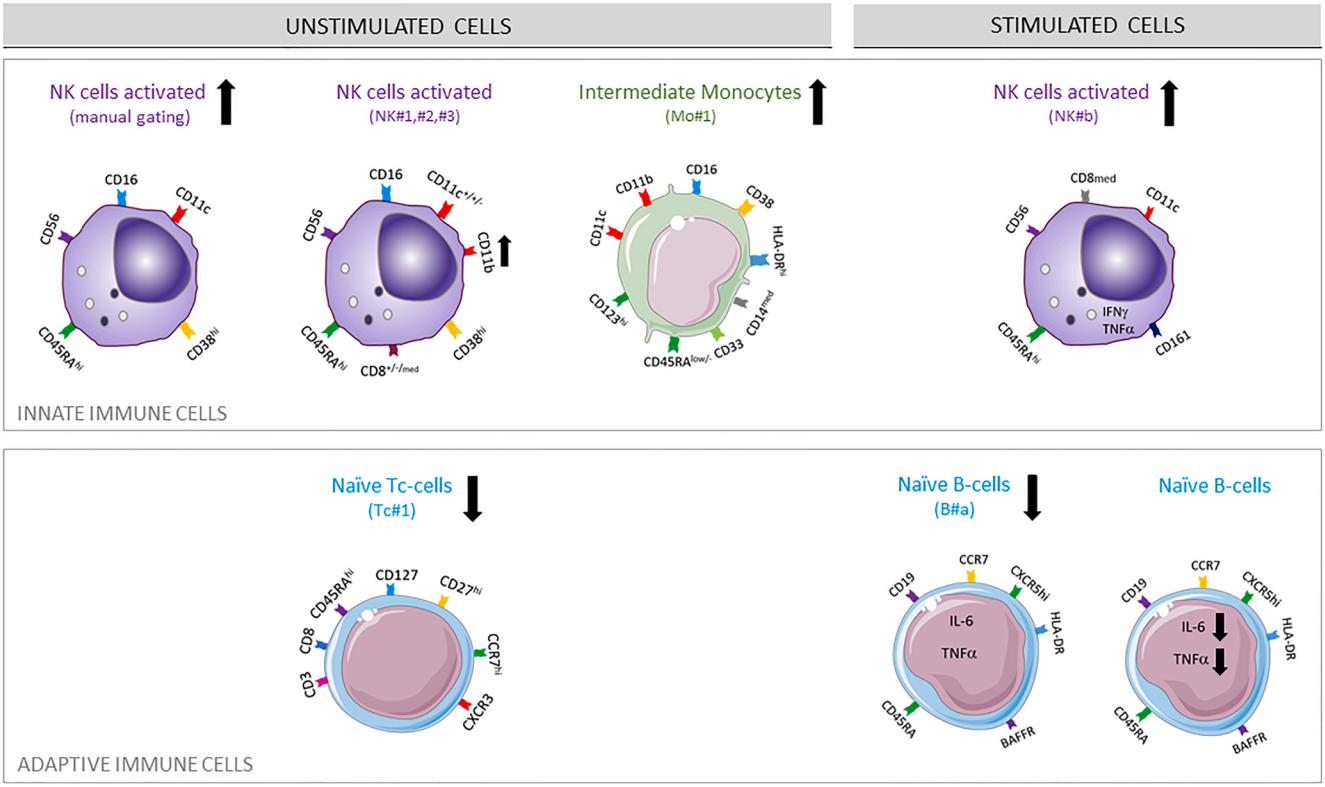

Fig. 7. An overview of the major cell populations associated with different ∑DEHP + DINP levels in the present study. Arrows illustrate statistically significantly increased or decreased cell subset abundancy or expression of the functional markers per cell, in the high versus the low ∑DEHP + DINP exposed group (n = 16). The surface markers and cytokines shown in the illustrations represent the characteristic marker expression pattern for the various cell populations of interest. The short names in parenthesis refer to the cell populations described in the CITRUS-trees and text of the results section.

manual gating of the overall Mo population. Multiple diseases, including bacterial and viral infections, autoimmunity, and chronic inflammation, are associated with changes in monocyte subsets. Intermediate monocytes are more abundant in bacterial sepsis, dengue fever, Crohn's disease, cardiovascular disease and rheumatoid arthritis (Thomas et al., 2017). The intermediate Mo population also expressed high levels of the inflammatory phenotypic markers CD11b and CD11c, shown to be upregulated in monocytes by factors like TNFα (Al-Rashed et al., 2019). Accordingly, phthalates have been reported to affect monocytes (Bølling et al., 2020; Hansen et al., 2015), although not these specific phenotypic markers. CD11b and CD11c, beta 2 integrins, are adhesins and activation markers, both contributing to and regulating immune responses (Schittenhelm et al., 2017). Their gene expression (ITGAM-ITGAX) has been reported to be associated with autoimmune conditions like Systemic lupus erythematosus (Hom et al., 2008). Taken together, the consistent observations of increased abundance of activated NK cell subsets and monocytes along with increased cellular expression of pro-inflammatory markers are supporting and expanding previous evidence, and suggests that high phthalate exposure can promote a (low grade) pro-inflammatory state in innate immune cells. Thus, these innate cell populations deserve further exploration as target cells for phthalate exposure. For a more thorough assessment of the innate arm, fresh blood samples could be investigated, also including the granulocyte cell populations.

Among the adaptive cells, several clusters of Tc, Th, Tfh and B cells were identified in the CITRUS analyses. It is worth noting that although not strong or verified after manual gating for the T cell populations, the trends for both T and B cell clusters were all in the direction of lower abundancy in the high ∑DEHP + DiNP exposure group. The observation of lower percentages of TNFα and IL-6 double positive B cells in the high ∑DEHP + DiNP exposure group was robust. Cytokine-producing B cells have been reported to play a role in autoimmune diseases (Fleischer et al., 2015; Yilmaz et al., 2015), and IL-6 and TNFα are found to be important in B-cell function and proliferation (Rieckmann et al., 1997). Interestingly, a lack of B-cell derived IL-6 has been reported to prevent follicular helper T-cell (Tfh) differentiation (Arkatkar et al., 2017; Eto et al., 2011) and B cell-derived TNFα has been reported to be important for regulating other follicular cells (Lund, 2008). On the other hand, DEHP has been suggested to lead to expansion of Tfh cells, which modifies the functionality of antibody producing B cells in a mouse model for ovalbumin sensitization (Han et al., 2014). Although we did not see strong effects (but indeed tendencies) on circulating Tfh, the observed changes in the double positive B cells may reflect possible phthalate effects on Tfh cells in lymphoid tissues and thus may support a functional role of phthalates in disturbing Tfh-B cell interactions. Previous experimental studies suggested that phthalates enhanced allergen-induced responses in mice, including a shift towards Th2 and Th17 responses, while in vitro studies report modulation of dendritic cell differentiation and T cell interaction, also with increased release of Th2 mediators (Bølling et al., 2020). However, no associations were observed between ∑DEHP + DiNP levels and T cell cytokine production or Th2/Th17 marker expression in the current analysis. This discrepancy is most likely due to our experimental design, with application of the general (and not allergen-specific) cellular stimuli PMA/ionomycin.

The strength of the high-dimensional mass cytometry approach is the high number of markers allowing combination of a detailed immune cell phenotyping with surface markers with numerous functional markers like activation markers and intracellular cytokines on a single cell level. Overall, the markers identified to differ between groups were in general functional markers, such as combined cytokine production (polyfunctional cells) and expression of activation or maturation markers. This suggest that functional markers, rather than traditional cell phenotyping, are more sensitive for revealing associations with phthalate exposure. Thus, polyfunctionality and activation markers like the ones

identified in the present study deserve further investigation as biomarkers for effect as well as for improved mechanistic knowledge. It should be noted, however, that use of PBMCs going through a freeze–thaw cycle as in the present study may affect certain phenotype and functional markers, while this cell storage step also assures high degree of standardized preservation and high reproducibility (Martikainen and Roponen, 2020). The application of high-dimensional cytometry will be important to achieve simultaneous detection of cell types and combination of functional markers.

One of the strengths of the present study is the accuracy in the individual exposure levels, due to measurements of several specific metabolites over a 24-hour period (Husoy et al., 2019), integrating all routes of exposure and bioavailability. Since half-lives of the metabolites are relatively short, the urinary levels over this 24-hour period directly preceding the collection of the PBMCs can be considered a good reflection of the actual exposure. Thus, the associations between exposure level and the immune cell profiles may reflect acute, as opposed to chronic, effects from exposure during the latest 24-hour period. However, we cannot exclude that the associations also may be caused by chronic exposure to similar levels of phthalates over time due to similar lifestyle patterns and widespread use of phthalates resulting in a continuous exposure to phthalates. Metabolite analysis of a second 24-hour urine pool from the same subjects collected after a 2–3 week interval gave similar concentrations of DEHP metabolites as for the presented levels (Husøy et al, in press). Also, contribution from other, confounding environmental exposures or lifestyle factors cannot be excluded, although the selection of participants was performed to reduce influence from other xenobiotics in the high phthalate group. Experimental studies in vivo or in vitro with controlled exposure are required to confirm causality.

Sex-dependent effects of phthalates have been reported for asthma and allergy-related diseases (Buckley et al., 2018; Hoppin et al., 2004; Ku et al., 2015; Soomro et al., 2018) and may be linked to their endocrine-disrupting capacities (Chalubinski and Kowalski, 2006). Although the power in the present study was too low to reach significances when stratifying by sex, some of the cell clusters identified by the CITRUS analyses appeared to be more strongly affected in one of the sexes. This may suggest that some of the observed associations between phthalate levels and altered immune cell profiles may be influenced by or interact with the endocrine-disrupting mechanisms.

5. Conclusions

This exploratory study assessing cell subset percentages and expression of functional markers suggests that DEHP and DiNP phthalate exposure may stimulate particular subsets of innate immune cells while suppressing certain adaptive immune cell subsets. Monocytes and TNFα + IFNγ + CD11c + activated NK cells, as well as IL-6 + TNFα + B cells were the populations showing the most consistent differences between the high and low phthalate exposure groups. Several of these cell characteristics have also been linked to immune diseases. Experimental studies of phthalate-induced effects in NK and B cells are virtually lacking in the literature but the present data suggest that further studies of impact on these cell types are warranted. By revealing significant immunological differences even between small groups, this study illustrates the promise of the broad and deep information obtained by high-dimensional single cell analyses of human samples to answer toxicological research questions and to suggest novel mechanistic pathways and biomarkers of effect. It is highly recommended that PBMCs are collected in future biomonitoring studies to verify and exploit this approach.

CRediT authorship contribution statement

Unni C. Nygaard: Conceptualization, Data curation, Formal analysis, Methodology, Supervision, Writing - original draft. **Emilie S. Ulriksen:** Investigation, Data curation, Formal analysis, Writing - original draft. **Hege Hjertholm:** Investigation, Project administration, Methodology. **Friederike Sonnet:** Data curation, Methodology, Supervision. **Anette K. Bølling:** Data curation. **Monica Andreassen:** Conceptualization, Project administration. **Trine Husøy:** Conceptualization, Funding acquisition, Resources. **Hubert Dirven:** Conceptualization, Funding acquisition, Resources.

Declaration of Competing Interest

The authors declare that they have no known competing financial interests or personal relationships that could have appeared to influence the work reported in this paper.

Acknowledgements

The authors want to acknowledge the NIPH EuroMix study team for performing the collection of samples used for exposure and immune cell profiling. We further want to thank all volunteers for their participation in the study.

Funding

The present study was funded by the Norwegian Institute of Public Health, while collection of samples and phthalate exposure assessment in The EuroMix project was funded by the Horizon 2020 Framework Program of the European Union (Grant Agreement 633172 – EuroMix) coordinated by Jacob van Klaveren (RIVM, the Netherlands). The funding sources did not influence the study design, data collection, analyses and interpretation of the data.

Appendix A. Supplementary material

Supplementary data to this article can be found online at https://doi.org/10.1016/j.envint.2020.106283.

References

Agier, L., Basagaña, X., Maitre, L., Granum, B., Bird, P.K., Casas, M., et al., 2019. Early-life exposome and lung function in children in Europe: An analysis of data from the longitudinal, population-based helix cohort. The Lancet Planetary Health 3, e81–e92.

Al-Rashed, F., Ahmad, Z., Iskandar, M.A., Tuomilehto, J., Al-Mulla, F., Ahmad, R., 2019. Tnf-α induces a pro-inflammatory phenotypic shift in monocytes through acsl1: Relevance to metabolic inflammation. Cell. Physiol. Biochem. 52, 397–407.

Alfardan, A.S., Nadeem, A., Ahmad, S.F., Al-Harbi, N.O., Al-Harbi, M.M., AlSharari, S.D., 2018. Plasticizer, di(2-ethylhexyl)phthalate (dehp) enhances cockroach allergen extract-driven airway inflammation by enhancing pulmonary th2 as well as th17 immune responses in mice. Environ. Res. 164, 327–339.

Amir el, A.D., Davis, K.L., Tadmor, M.D., Simonds, E.F., Levine, J.H., Bendall, S.C., et al., 2013. Visne enables visualization of high dimensional single-cell data and reveals phenotypic heterogeneity of leukemia. Nat. Biotechnol. 31, 545–552.

Aranami, T., Miyake, S., Yamamura, T., 2006. Differential expression of cd11c by peripheral blood nk cells reflects temporal activity of multiple sclerosis. J. Immunol. 177, 5659–5667.

Arkatkar, T., Du, S.W., Jacobs, H.M., Dam, E.M., Hou, B., Buckner, J.H., et al., 2017. B cell-derived il-6 initiates spontaneous germinal center formation during systemic autoimmunity. J. Exp. Med. 214, 3207–3217.

Baken, K.A., Lambrechts, N., Remy, S., Mustieles, V., Rodríguez-Carrillo, A., Neophytou, C.M., et al., 2019. A strategy to validate a selection of human effect biomarkers using adverse outcome pathways: Proof of concept for phthalates and reproductive effects. Environ. Res. 175, 235–256.

Bandura, D.R., Baranov, V.I., Ornatsky, O.I., Antonov, A., Kinach, R., Lou, X., et al., 2009. Mass cytometry: Technique for real time single cell multitarget immunoassay based on inductively coupled plasma time-of-flight mass spectrometry. Anal. Chem. 81, 6813–6822.

Barcenilla, H., Åkerman, L., Pihl, M., Ludvigsson, J., Casas, R., 2019. Mass cytometry identifies distinct subsets of regulatory t cells and natural killer cells associated with high risk for type 1 diabetes. Front. Immunol. 10, 982.

Bendall, S.C., Nolan, G.P., Roederer, M., Chattopadhyay, P.K., 2012. A deep profiler's guide to cytometry. Trends Immunol. 33, 323–332.

Bendall, S.C., Davis, K.L., Amir el, A.D., Tadmor, M.D., Simonds, E.F., Chen, T.J., et al., 2014. Single-cell trajectory detection uncovers progression and regulatory coordination in human b cell development. Cell 157, 714–725.

Bolling, A.K., Holme, J., Bornehag, C.G., Nygaard, U.C., Bertelsen, R.J., Nånberg, E., et al., 2013. Pulmonary phthalae exposure and asthma - is ppar a plausible mechanistic link? EXCLI J. 2013 (12), 26.
Bruggner, R.V., Bodenmiller, B., Dill, D.L., Tibshirani, R.J., Nolan, G.P., 2014. Automated identification of stratifying signatures in cellular subpopulations. PNAS 111, E2770–E2777.
Buckley, J.P., Quirós-Alcalá, L., Teitelbaum, S.L., Calafat, A.M., Wolff, M.S., Engel, S.M., 2018. Associations of prenatal environmental phenol and phthalate biomarkers with respiratory and allergic diseases among children aged 6 and 7 years. Environ. Int. 115, 79–88.
Bølling, A.K., Sripada, K., Becher, R., Bekö, G., 2020. Phthalate exposure and allergic diseases: Review of epidemiological and experimental evidence. Environ. Int. 139, 105706.
Cahill, L.A., Guo, F., Nguyen, J., Zhang, F., Seshadri, A., Keegan, J., et al., 2020. Circulating factors in trauma plasma activate specific human immune cell subsets. Injury.
Chalubinski, M., Kowalski, M.L., 2006. Endocrine disrupters–potential modulators of the immune system and allergic response. Allergy 61, 1326–1335.
Chen, L., Chen, J., Xie, C.M., Zhao, Y., Wang, X., Zhang, Y.H., 2015. Maternal disononyl phthalate exposure activates allergic airway inflammation via stimulating the phosphoinositide 3-kinase/akt pathway in rat pups. Biomed. Environ. Sci. 28, 190–198.
Davis, M.M., Tato, C.M., Furman, D., 2017. Systems immunology: Just getting started. Nat. Immunol. 18, 725–732.
Duan, J., Deng, T., Kang, J., Chen, M., 2019. Dinp aggravates autoimmune thyroid disease through activation of the akt/mtor pathway and suppression of autophagy in wistar rats. Environ. Pollut. 245, 316–324.
EFSA CEF Panel (EFSA Panel on Food Contact Materials E, Flavourings and Processing Aids), Silano V, Barat Baviera JM, Bolognesi C, Chesson A, Cocconcelli PS, et al., 2019. Scientific opinion on the update of the risk assessment of di-butylphthalate (dbp), butyl-benzyl-phthalate (bbp), bis(2-ethylhexyl)phthalate (dehp), di-isononylphthalate (dinp) and di-isodecylphthalate (didp) for use in food contact materials. EFSA J 17:85.
Eljezi, T., Pinta, P., Nativel, F., Richard, D., Pinguet, J., Roy, O., et al., 2019. In vitro cytotoxic effects of secondary metabolites of dehp and its alternative plasticizers dinch and dinp on a l929 cell line. Int. J. Hyg. Environ. Health 222, 583–589.
Eto, D., Lao, C., DiToro, D., Barnett, B., Escobar, T.C., Kageyama, R., et al., 2011. Il-21 and il-6 are critical for different aspects of b cell immunity and redundantly induce optimal follicular helper cd4 t cell (tfh) differentiation. PLoS ONE 6, e17739.
Fleischer, V., Sieber, J., Fleischer, S.J., Shock, A., Heine, G., Daridon, C., et al., 2015. Epratuzumab inhibits the production of the proinflammatory cytokines il-6 and tnf-α, but not the regulatory cytokine il-10, by b cells from healthy donors and sle patients. Arthritis Res. Ther. 17, 185.
Freud, A.G., Yokohama, A., Becknell, B., Lee, M.T., Mao, H.C., Ferketich, A.K., et al., 2006. Evidence for discrete stages of human natural killer cell differentiation in vivo. J. Exp. Med. 203, 1033–1043.
Fu, B., Tian, Z., Wei, H., 2014. Subsets of human natural killer cells and their regulatory effects. Immunology 141, 483–489.
Grace, C., Nacheva, E.P., 2012. Significance analysis of microarrays (sam) offers clues to differences between the genomes of adult philadelphia positive all and the lymphoid blast transformation of cml. Cancer Inform 11, 173–183.
Guo, J., Han, B., Qin, L., Li, B., You, H., Yang, J., et al., 2012. Pulmonary toxicity and adjuvant effect of di-(2-exylhexyl) phthalate in ovalbumin-immunized balb/c mice. PLoS ONE 7, e39008.
Han, Y., Wang, X., Chen, G., Xu, G., Liu, X., Zhu, W., et al., 2014. Di-(2-ethylhexyl) phthalate adjuvantly induces imbalanced humoral immunity in ovalbumin-sensitized balb/c mice ascribing to t follicular helper cells hyperfunction. Toxicology 324, 88–97.
Hansen, J.F., Bendtzen, K., Boas, M., Frederiksen, H., Nielsen, C.H., Rasmussen, Å.K., et al., 2015. Influence of phthalates on cytokine production in monocytes and macrophages: A systematic review of experimental trials. PLoS ONE 10, e0120083.
Hessel, E.V., Tonk, E.C., Bos, P.M., van Loveren, H., Piersma, A.H., 2015. Developmental immunotoxicity of chemicals in rodents and its possible regulatory impact. Crit. Rev. Toxicol. 45, 68–82.
Hom, G., Graham, R.R., Modrek, B., Taylor, K.E., Ortmann, W., Garnier, S., et al., 2008. Association of systemic lupus erythematosus with c8orf13-blk and itgam-itgax. N. Engl. J. Med. 358, 900–909.
Hoppin, J.A., Ulmer, R., London, S.J., 2004. Phthalate exposure and pulmonary function. Environ. Health Perspect. 112, 571–574.
Husoy, T., Andreassen, M., Hjertholm, H., Carlsen, M.H., Norberg, N., Sprong, C., et al., 2019. The norwegian biomonitoring study from the eu project euromix: Levels of phenols and phthalates in 24-hour urine samples and exposure sources from food and personal care products. Environ. Int. 132, 105103.
Kravchenko, J., Corsini, E., Williams, M.A., Decker, W., Manjili, M.H., Otsuki, T., et al., 2015. Chemical compounds from anthropogenic environment and immune evasion mechanisms: Potential interactions. Carcinogenesis 36 (Suppl 1), S111–S127.
Ku, H.Y., Su, P.H., Wen, H.J., Sun, H.L., Wang, C.J., Chen, H.Y., et al., 2015. Prenatal and postnatal exposure to phthalate esters and asthma: A 9-year follow-up study of a taiwanese birth cohort. PLoS ONE 10, e0123309.
Kurioka, A., Cosgrove, C., Simoni, Y., van Wilgenburg, B., Geremia, A., Bjorkander, S., et al., 2018. Cd161 defines a functionally distinct subset of pro-inflammatory natural killer cells. Front. Immunol. 9, 486.
Li, W., Okuda, A., Yamamoto, H., Yamanishi, K., Terada, N., Yamanishi, H., et al., 2013. Regulation of development of cd56brightcd11c+ nk-like cells with helper function by il-18. PLoS ONE 8, e82586.
Lund, F.E., 2008. Cytokine-producing b lymphocytes-key regulators of immunity. Curr. Opin. Immunol. 20, 332–338.
Luo, Q., Liu, Z.H., Yin, H., Dang, Z., Wu, P.X., Zhu, N.W., et al., 2018. Migration and potential risk of trace phthalates in bottled water: A global situation. Water Res. 147, 362–372.
Mahapatra, S., Shearer, W.T., Minard, C.G., Mace, E., Paul, M., Orange, J.S., 2019. Nk cells in treated hiv-infected children display altered phenotype and function. J. Allergy Clin. Immunol. 144, 294–303.e213.
Martikainen, M.V., Roponen, M., 2020. Cryopreservation affected the levels of immune responses of pbmcs and antigen-presenting cells. Toxicol. In Vitro 67, 104918.
Michel, T., Poli, A., Cuapio, A., Briquemont, B., Iserentant, G., Ollert, M., et al., 2016. Human cd56bright nk cells: An update. J. Immunol. 196, 2923–2931.
Rieckmann, P., Tuscano, J.M., Kehrl, J.H., 1997. Tumor necrosis factor-alpha (tnf-alpha) and interleukin-6 (il-6) in b-lymphocyte function. Methods 11, 128–132.
Sabaredzovic, A., Sakhi, A.K., Brantsaeter, A.L., Thomsen, C., 2015. Determination of 12 urinary phthalate metabolites in norwegian pregnant women by core-shell high performance liquid chromatography with on-line solid-phase extraction, column switching and tandem mass spectrometry. J. Chromatogr., B: Anal. Technol. Biomed. Life Sci. 1002, 343–352.
Schittenhelm, L., Hilkens, C.M., Morrison, V.L., 2017. B(2) integrins as regulators of dendritic cell, monocyte, and macrophage function. Front. Immunol. 8, 1866.
Sonnet, F., Namork, E., Stylianou, E., Gaare-Olstad, I., Huse, K., Andorf, S., et al., 2020. Reduced polyfunctional t cells and increased cellular activation markers in adult allergy patients reporting adverse reactions to food. BMC Immunol 21, 43.
Soomro, M.H., Baiz, N., Philippat, C., Vernet, C., Siroux, V., Nichole Maesano, C., et al., 2018. Prenatal exposure to phthalates and the development of eczema phenotypes in male children: Results from the eden mother-child cohort study. Environ. Health Perspect. 126, 027002.
Thomas, G.D., Hamers, A.A.J., Nakao, C., Marcovecchio, P., Taylor, A.M., McSkimming, C., et al., 2017. Human blood monocyte subsets: A new gating strategy defined using cell surface markers identified by mass cytometry. Arterioscler. Thromb. Vasc. Biol. 37, 1548–1558.
Tibshirani, R., 1996. Regression shrinkage and selection via the lasso. J. Royal Stat. Soc. Ser. B (Methodol.) 58, 22.
Tibshirani, R., Hastie, T., Narasimhan, B., Chu, G., 2002. Diagnosis of multiple cancer types by shrunken centroids of gene expression. PNAS 99, 6567–6572.
U.S. Department of Health and Human Services C, 2019. Fourth national report on human exposure to environmental chemicals, updated tables, january 2019. Centers for Disease Control and Prevention (CDC), Atlanta, GA.
Van der Laan, M., Pollard, K., Bryan, J., 2003. A new partitioning around medoids algorithm. J. Stat. Comput. Simul. 73, 575–584.
Vendrame, E., Fukuyama, J., Strauss-Albee, D.M., Holmes, S., Blish, C.A., 2017. Mass cytometry analytical approaches reveal cytokine-induced changes in natural killer cells. Cytometry, Part B 92, 57–67.
Wang, Y., Zhu, H., Kannan, K., 2019. A review of biomonitoring of phthalate exposures. Toxics 7.
Wittassek, M., Koch, H.M., Angerer, J., Brüning, T., 2011. Assessing exposure to phthalates - the human biomonitoring approach. Mol. Nutr. Food Res. 55, 7–31.
Wu, W., Wu, C., Ji, C., Diao, F., Peng, J., Luo, D., et al., 2020. Association between phthalate exposure and asthma risk: A meta-analysis of observational studies. Int. J. Hyg. Environ. Health 228, 113539.
Yilmaz, V., Oflazer, P., Aysal, F., Parman, Y.G., Direskeneli, H., Deymeer, F., et al., 2015. B cells produce less il-10, il-6 and tnf-α in myasthenia gravis. Autoimmunity 48, 201–207.